Research Square

Preprints are preliminary reports that have not undergone peer review.
They should not be considered conclusive, used to inform clinical practice,
or referenced by the media as validated information.

Investigating Fracture of Ti-6Al-4V Tensile Specimens Manufactured by Electron Beam Powder Bed Fusion Using XFEM

Bahman Paygozar

bpaygozar@etu.edu.tr

TOBB University of Economics and Technology

Research Article

Keywords: Electron beam powder bed fusion, Dogbone specimen, Extended finite element method, Fracture load

Posted Date: April 14th, 2026

DOI: https://doi.org/10.21203/rs.3.rs-9396217/v1

License: This work is licensed under a Creative Commons Attribution 4.0 International License.
Read Full License

Additional Declarations: No competing interests reported.

Investigating Fracture of Ti-6Al-4V Tensile Specimens Manufactured by Electron Beam Powder Bed Fusion Using XFEM

Abstract: This study aims to reliably predict the fracture load of the rectangular Ti-6Al-4V dogbone specimen fabricated by electron beam powder bed fusion (EB-PBF). Tensile tests were conducted, and corresponding numerical simulations were performed. The experimental data obtained from standard tensile tests were used to extract the mechanical properties of the material. Subsequently, the load-displacement responses from the experiments were used to calibrate the fracture properties for use in failure analyses performed using the extended finite element method (XFEM) by comparing the corresponding numerical and experimental results. This calibration process ensured that the model realistically represents damage initiation and evolution. It was also shown that the XFEM approach successfully captures crack initiation and propagation. The data (e.g., stiffness and fracture load) obtained from experimental tensile tests were compared with the results of numerical analyses. The discrepancy between the numerical and experimental results was within an acceptable range (below 5%) for the dogbone specimen. These findings highlighted the potential of XFEM as a reliable tool for predicting the fracture behavior of EB-PBF-produced specimens under tensile loading.

Keywords: Electron beam powder bed fusion; Dogbone specimen; Extended finite element method; Fracture load.

1. Introduction

Titanium alloys are widely used in the aerospace, biomedical, and energy sectors, particularly due to their superior properties, such as high specific strength, excellent corrosion resistance, and biocompatibility [1]. Among these alloys, Ti-6Al-4V is one of the most preferred materials in the industry, notable for both its mechanical performance and manufacturability. Ti-6Al-4V parts obtained through traditional production methods generally undergo forging or machining processes, which makes the production of complex geometries difficult and also leads to material waste. At this point, additive manufacturing technologies stand out as a significant alternative, particularly given the advantages they provide in fabricating complex geometries [2, 3].

Electron Beam Powder Bed Fusion (EB-PBF) is an advanced additive manufacturing technique in which metal powders are selectively melted using a high-energy electron beam. This method is utilized in fabricating components for various industries, including biomedical [4], automotive [5], and aeronautics [6], made of different materials. For example, Ti-6Al-4V parts produced by the EB-PBF method are notable for their fine microstructures, low residual stresses, and suitable mechanical performance [7]. Hence, it does not require any additional heat-treatment procedure to modify the microstructure [8]. However, factors such as anisotropy, porosity, and microstructural heterogeneity, which are specific to the additive manufacturing process, directly affect the mechanical behavior of these parts [9]. Additionally, controlling defects that occur during the AM procedure is another challenge. These defects can negatively affect the fatigue life, tensile, and fracture behavior of the material. Especially under tensile loads, these defects can act as crack initiation points, causing a premature fracture. Hence, conducting a detailed investigation of the mechanical behavior of tensile specimens produced by the EB-PBF method is so important. In this context, tensile tests are one of the fundamental mechanical tests widely used to determine the elastic and plastic deformation behavior, yield strength, maximum tensile strength, and elongation at fracture of a material [10]. These tests provide important information about the material's performance under service conditions. However, relying solely on experimental data makes it difficult to fully understand complex damage mechanisms, especially crack formation and propagation [11]. Therefore, the combined use of both experimental and numerical methods allows for a more accurate understanding of the material's behavior.

The Extended Finite Element Method (XFEM) is a powerful numerical analysis method developed for modeling crack formation and propagation. Compared to conventional finite

element methods [12, 13], the XFEM technique facilitates the identification and propagation of cracks without being limited by their mesh structure [14, 15]. This feature provides a significant advantage, particularly in modeling complex crack geometries and heterogeneous structures within materials. XFEM can accurately represent stress concentrations at crack tips and offers high accuracy in fracture mechanics analyses [16]. For example, Verma et al. [15] investigated the tensile, fracture toughness, and fatigue crack growth behavior of additively manufactured Ti6Al4V alloy using the XFEM technique.

Given the literature, it was found that there are few studies investigating the failure of components fabricated by EB-PBF using the finite element approach [15, 17, 18], particularly regarding the use of the XFEM technique and tensile behavior. In this regard, the main objective of this study is to investigate the mechanical properties of Ti-6Al-4V tensile specimens produced by the EB-PBF method through both experimental characterization and numerical analysis, thereby addressing a gap in the literature. In this context, the elastic and plastic deformation properties of the material are determined using data obtained from tensile tests, and damage evolution and crack propagation are modeled using the XFEM method numerically. The experimental load-displacement results were utilized to calibrate the numerical analyses and the material properties employed therein. The calibration procedure takes into account the defects that might have been introduced during the fabrication process. The results obtained in this study are expected to contribute to the design of Ti-6Al-4V components subjected to tensile loading in engineering fields such as aerospace and automotive applications.

2. Experimental investigations

The tensile specimens were manufactured with dimensions mentioned in the ASTM E8 standard, as shown in Fig. 1. The samples were fabricated in the rectangular configuration using the EB-PBF method with the ARCAM EBM A2X machine. Some of the process parameters are given in Table 1.

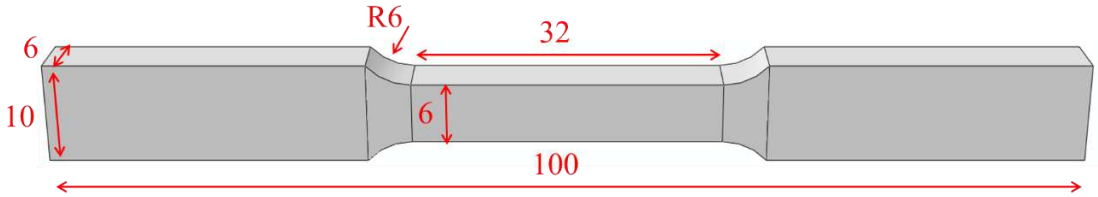


Fig. 1. Configuration of the tensile specimen as per standard ASTM-E8. All dimensions are mentioned in mm.

Table 1. Process parameters used for the fabrication of samples [19].

Process parameters	Quantity
Hatch spacing [μm]	150
Spot size [μm]	200
Layer thickness [μm]	50
Scanning speed [mm/s]	4530
Focus offset [mA]	3
Pre-heat temperature [°C]	700

The manufactured samples, in standard dimensions, were subjected to tensile testing on a universal testing machine (Instron 600 DX, USA). The test speed was selected as 1 mm/min, based on the ASTM E8 standard. The load-displacement responses of the specimens were extracted for later use in validating the numerical results.

3. Numerical investigations

3.1. Extended finite element method

To simulate the fracture, the XFEM technique was used in this study. It is a numerical approach capable of handling discontinuities such as cracks, thereby facilitating the simulation of material fracture behavior (e.g., crack propagation) [20, 21]. The XFEM enables the crack to propagate through the element interior by incorporating enrichment functions into the conventional FE method [22]. It also predicts crack propagation in additively manufactured parts [21, 23]. The enrichment functions in XFEM facilitate displacement jumps across crack faces and model the singularity at the crack tip [24]. The discretized displacement field, u^h in XFEM [25], is defined by

$$u^h_{(x)} = \sum_{i\epsilon N} N_i(x)\left[u_i + H(x)a_i + \sum_{j=1}^{4} F_j(x)b_i^j\right] \quad (1)$$

where N_i and u_i are the blending function and the nodal displacement vector, respectively. The $H(x)a_i$ indicates a Heaviside enrichment, and $\sum_{j=1}^{4} F_j(x)b_i^j$ shows crack tip enrichment. The superscripts i and j demonstrate the node number and the enrichment function's number at the crack front, respectively. Also, $H(x)$ indicates the Heaviside distribution, a_i reflects the enriched nodal degree of freedoms for the elements cut through the crack (i.e., jump

discontinuity). $F_j(x)$ and b_i^j are respectively referred to as the crack tip asymptotic function and the crack tip enriched nodal degree of freedom [26].

The crack initiation and propagation processes in XFEM were modeled by a cohesive traction-separation law [27, 28]. To use the linear type of traction-separation law, the maximum principal stress (MaxPS) criterion was selected in this study to model the crack initiation [29, 30]. According to this criterion, when the maximum principal stress (σ_p) experienced in an element reaches the ultimate strength (σ_u) of the material, the material starts to fail from that element. The failure equation is given by.

$$\frac{\sigma_p}{\sigma_u} = 1 \tag{2}$$

Fracture energy power-law criteria in 3D versions can be used to model crack propagation through damage evolution [28, 30].

$$\left\{\frac{G_n}{G_n^C}\right\} + \left\{\frac{G_s}{G_s^C}\right\} + \left\{\frac{G_t}{G_t^C}\right\} = 1 \tag{3}$$

where, G_n, G_s, and G_t are strain energy release rates (i.e., fracture energies) in normal, first, and second shear directions concerning the interface, respectively. Superscript *C*, added to the previous parameters, reflects their critical values. Considering the experimental investigations of this study, i.e., dealing with either pure Mode I, only the first term of the equation above will be active on the left-hand side. It is worth noting that the critical mode I fracture energy can be found using Eq. (4) and mode I fracture toughness. The symbols E and ν denote the material's Young's modulus and Poisson's ratio, respectively.

$$G_n^C = G_{Ic} = \frac{K_I^2(1-\nu^2)}{E} \tag{4}$$

3.2. Numerical simulations

The rectangular dogbone specimen was modeled three-dimensionally in ABAQUS, as shown in Fig. 2. To capture the damage and failure of the sample, the XFEM technique was employed. The defined crack propagation domain is shown in Fig. 2(a) by green cross symbols. The MaxPS and Power Law criteria were implemented to capture the crack initiation and propagation in the model. The eight-node brick elements (signified by C3D8) were utilized in the numerical models, as shown in Fig. 2(b). As boundary conditions, all the DOFs of the specimen at both ends, except for the displacement of the top end in the loading direction, were

fully constrained. The loading on the specimen was applied by the displacement exerted at one end of the model in the XFEM analyses. The mechanical properties of Ti-6Al-4V, used in the numerical investigations, were obtained from the tensile experiments conducted in this study (Table 2). The fracture properties of the material were obtained from a similar study [31] and calibrated using the experimental load-displacement responses. In this regard, during the calibration process, the mode I fracture toughness was updated from 75.95 to 85.73 $MPa\sqrt{m}$. This can be justified by the fact that there are slight difference in the process parameters and the machine used in this study and the article published by Ninerola et al. [31].

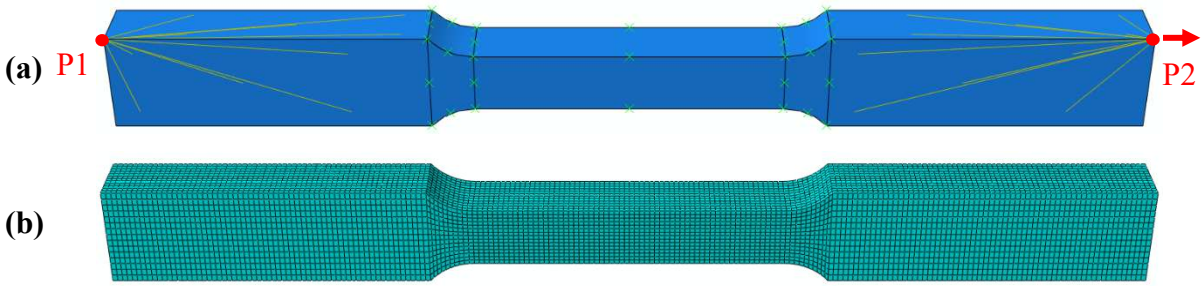


Fig. 2. Numerical model of the tensile rectangular specimens: (a) crack propagation domain and boundary conditions and (b) meshing pattern.

4. Results and discussion

4.1. Experimental results

After conducting the tensile tests on the dogbone specimens, the load-displacement curves were extracted; then, the data were changed to stress and strain values, as shown in Fig. 3. The mechanical properties of the specimens (i.e., peak load and stiffness) were obtained from the load-displacement responses, as listed in Table 2. The lower coefficients of variation (i.e., the standard deviation value divided by the average value) indicate the suitability and repeatability of the tests. The experimental and numerical failure of the specimen, as well as the crack propagation path, is later shown in Fig. 5.

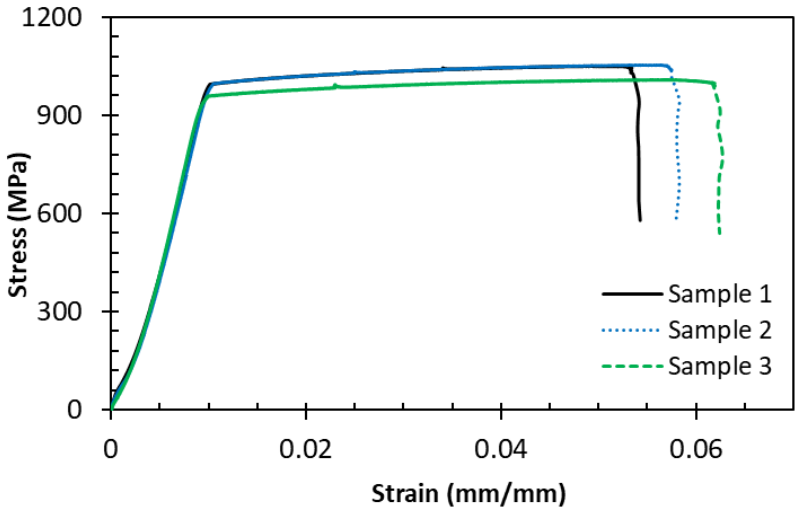


Fig. 3. Stress-strain responses of the tensile samples.

Table 2. Experimental data obtained from dogbone tensile tests.

Property	Sample 1	Sample 2	Sample 3	Avg.	St. Dev.	Coef. of variation (%)
Young's Modulus [GPa]	119.4	120.6	118.7	119.6	1.0	0.84
Yield Strength [MPa]	994	997	958.5	983.2	21.4	2.18
Tensile Strength [MPa]	1050.5	1053.9	1008.7	1037.7	25.2	2.43

4.2. Numerical results

The rectangular dogbone specimen modeled in ABAQUS was analyzed using the XFEM technique. A mesh refinement study was performed using the extracted mechanical and calibrated fracture material properties, and for four different element sizes, including 0.8, 0.6, 0.5, and 0.4 mm. Considering the computational costs and the difference between the load-displacement responses of different element sizes, it was revealed that a mesh size of 0.5 mm reflected suitable results. A comparison between the experimental results and numerical ones obtained using an element size of 0.5 was conducted, as shown in Fig. 4.

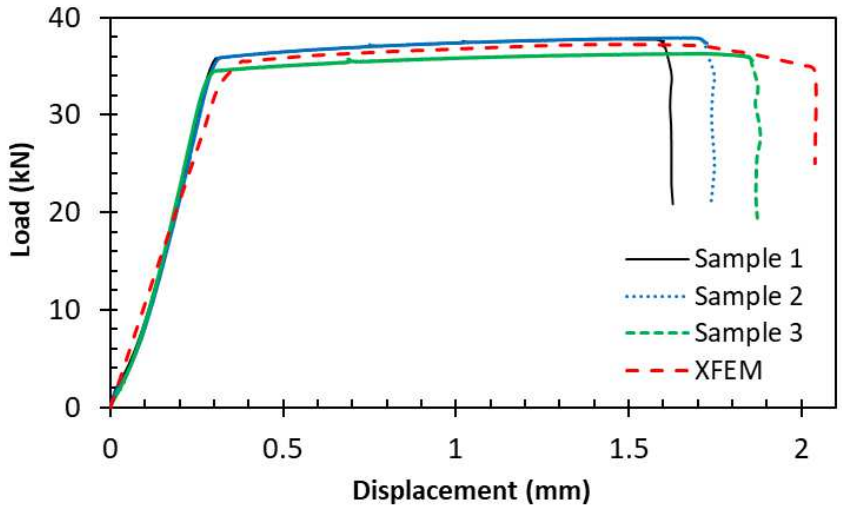
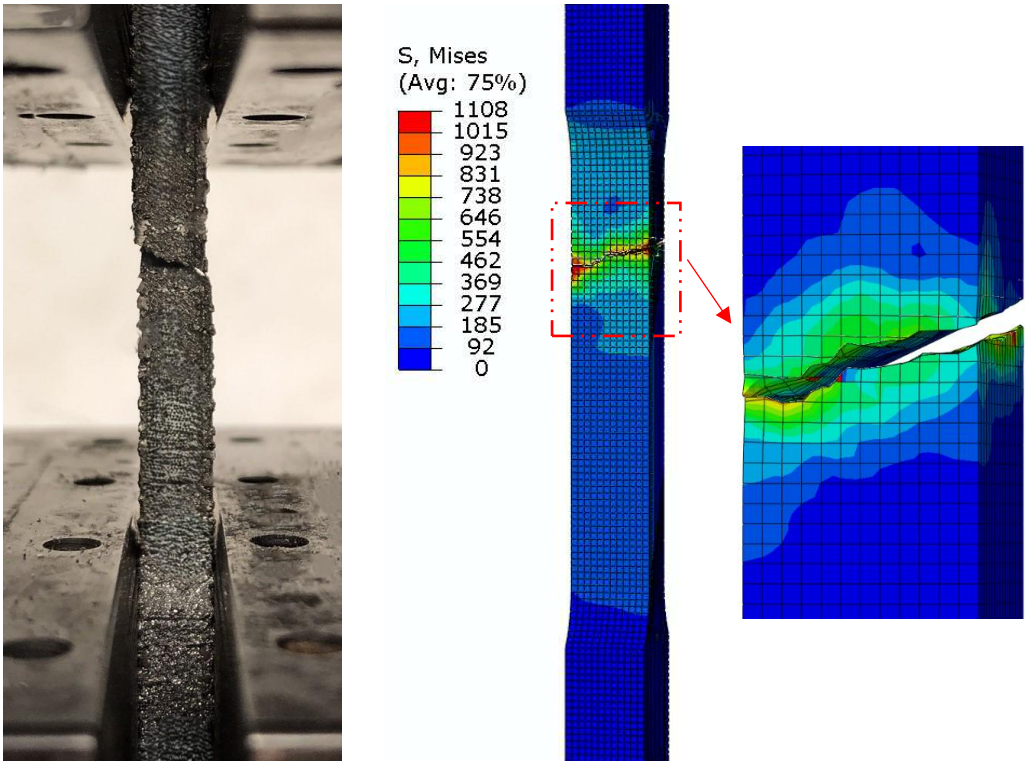


Fig. 4. Comparison between the experimental and numerical load-displacement responses of the tensile samples.

The failure and crack propagation in the specimen are shown in Fig. 5. It can be seen that there are similarities between the crack propagation and failure of the specimens. However, given the nature of EB-PBF, several tiny defects are always introduced during the fabrication of the specimens, whereas the numerical samples are modeled ideally without any defects. Taking into account the experimental and numerical results, the very close load-displacement responses (Fig. 4) and the similar failure patterns (Fig. 5), the simulation of the EB-PBF tensile specimens can be evaluated as successful.



(a) **(b)** **(c)**

Fig. 5. The failure and crack propagation in the (a) experimental sample and the numerical dogbone specimen (b) before and (c) after complete failure.

5. Conclusions

The tensile behavior and failure of the Ti-6Al-4V dogbone specimens fabricated by the EB-PBF technique were investigated experimentally and numerically using the XFEM technique. A comparison between experimental tensile test data and numerical predictions showed strong agreement, with differences remaining under 5% for the dogbone specimen. Overall, these outcomes and similar crack propagation paths confirm that XFEM is a dependable and effective approach for predicting the fracture behavior of EB-PBF-manufactured specimens subjected to tensile loading.

Conflict of Interest: The author declares that no known competing financial interests or personal relationships could have appeared to influence the work reported in this paper.

Data availability: The datasets generated during and/or analyzed during the current study are available from the author upon reasonable request.

Acknowledgment: The author would like to thank Dr. Firat Memu from TOBB University of Economics and Technology for conducting the experiments.

References:

1. Najafizadeh, M., et al., *Classification and applications of titanium and its alloys: A review.* Journal of Alloys and Compounds Communications, 2024. **3**: p. 100019.
2. Liu, S. and Y.C. Shin, *Additive manufacturing of Ti6Al4V alloy: A review.* Materials & Design, 2019. **164**: p. 107552.
3. Zhang, L.-N., et al., *Distinctive mechanical responses of strut-based and triply periodic minimal surface (TPMS) Ti-6Al-4V diamond lattice structures produced by electron beam melting.* Metals Advances, 2026. **41**: p. 45-54.
4. Tamayo, J.A., et al., *Additive manufacturing of Ti6Al4V alloy via electron beam melting for the development of implants for the biomedical industry.* Heliyon, 2021. **7**(5).
5. Juechter, V., et al., *Additive manufacturing of Ti-45Al-4Nb-C by selective electron beam melting for automotive applications.* Additive Manufacturing, 2018. **22**: p. 118-126.
6. Kovalchuk, D., V. Melnyk, and I. Melnyk, *A Coaxial Wire-Feed Additive Manufacturing of Metal Components Using a Profile Electron Beam in Space Application.* Journal of Materials Engineering and Performance, 2022. **31**(8): p. 6069-6082.
7. Davies, G.R., et al., *Influence of melt parameters on the microstructure of electron beam melted Ti–6Al–4V.* Journal of Materials Research and Technology, 2024. **32**: p. 3038-3046.
8. Saboori, A., et al., *Electron beam powder bed fusion of Ti–6Al–2Sn–4Zr–2Mo alloy: microstructure evolution and high-temperature mechanical properties.* Progress in Additive Manufacturing, 2025. **10**(9): p. 6627-6641.
9. Kok, Y., et al., *Anisotropy and heterogeneity of microstructure and mechanical properties in metal additive manufacturing: A critical review.* Materials & Design, 2018. **139**: p. 565-586.
10. Barbagallo, R., et al. *Study of the Electron Beam Melting Process Parameters' Influence on the Tensile Behavior of 3D Printed Ti6Al4V ELI Alloy in Static and Dynamic Conditions*. Materials, 2022. **15**, 4217 DOI: 10.3390/ma15124217.
11. Sepe, R., et al., *Correlation between real geometry and tensile mechanical behaviour for Ti6Al4V electron beam melted thin specimens.* Theoretical and Applied Fracture Mechanics, 2020. **107**: p. 102519.
12. Afroz, L., et al., *Analysing the effect of defects on stress concentration and fatigue life of L-PBF AlSi10Mg alloy using finite element modelling.* Progress in Additive Manufacturing, 2024. **9**(2): p. 341-359.
13. Dunbar, A.J., et al., *Experimental validation of finite element modeling for laser powder bed fusion deformation.* Additive Manufacturing, 2016. **12**: p. 108-120.
14. Verma, R., et al., *Fracture toughness and fatigue crack growth behaviour of laser powder bed fusion (LPBF) built Ti-6Al-4V alloy through XFEM.* Procedia Structural Integrity, 2023. **46**: p. 175-181.

15. Verma, R., et al., *Extended finite element simulation on Tensile, fracture toughness and fatigue crack growth behaviour of additively manufactured Ti6Al4V alloy.* Theoretical and Applied Fracture Mechanics, 2022. **117**: p. 103163.
16. Hu, Y., *Computational mechanics of crack growth in selective laser sintering by means of eXtend finite element method (XFEM)*. 2021, University of Sheffield.
17. Yılmaz, F., *Mechanical Characterization of Additively Manufactured Ti-6Al-4V Aircraft Structural Components Produced by Electron Beam Melting*. 2022, Middle East Technical University (Turkey).
18. Arrieta, E., *Comprehensive finite element modeling of Ti-6Al-4V cellular solids fabricated by electron beam melting*. 2017: The University of Texas at El Paso.
19. Arslan Bin Riaz, M., H.İ. Erten, and M. Güden, *Novel strut-based mechanical analysis: flow stress determination of electron beam melt (EBM) lattice structures.* Progress in Additive Manufacturing, 2025. **10**(12): p. 10505-10514.
20. Ghandriz, R., K. Hart, and J. Li, *Extended finite element method (XFEM) modeling of fracture in additively manufactured polymers.* Additive Manufacturing, 2020. **31**: p. 100945.
21. Akhavan-Safar, A., et al., *Mixed mode I/III fracture behavior of adhesive joints.* International Journal of Solids and Structures, 2020. **199**: p. 109-119.
22. Paygozar, B. and R.M. Gorguluarslan, *Numerical Investigation on Mode I and Mode II Fracture in Additively Manufactured PLA Material Using XFEM.* Journal of Polymer Science, 2026. **64**(4): p. 941-957.
23. Mubashar, A., I.A. Ashcroft, and A.D. Crocombe, *Modelling Damage and Failure in Adhesive Joints Using A Combined XFEM-Cohesive Element Methodology.* The Journal of Adhesion, 2014. **90**(8): p. 682-697.
24. Stein, N., et al., *Enhanced XFEM for crack deflection in multi-material joints.* International Journal of Fracture, 2017. **207**(2): p. 193-210.
25. Biswakarma, J.J.S., et al., *Modeling Brittle Fractures in Epoxy Nanocomposites Using Extended Finite Element and Cohesive Zone Surface Methods.* Polymers, 2021. **13**(19): p. 3387.
26. Giner, E., et al., *An Abaqus implementation of the extended finite element method.* Engineering Fracture Mechanics, 2009. **76**(3): p. 347-368.
27. Paygozar, B. and R.M. Gorguluarslan, *Investigating Failure Behavior of Adhesive Joints with Dissimilar Materials of Steel and Additively Manufactured PLA.* Transactions of the Indian Institute of Metals, 2023. **76**(11): p. 3041-3048.
28. Elices, M., et al., *The cohesive zone model: advantages, limitations and challenges.* Engineering Fracture Mechanics, 2002. **69**(2): p. 137-163.
29. Campilho, R.D.S.G., et al., *eXtended Finite Element Method for fracture characterization of adhesive joints in pure mode I.* Computational Materials Science, 2011. **50**(4): p. 1543-1549.
30. Paygozar, B., et al., *Adhesively bonded aluminium double-strap joints: effects of patch part on failure load.* Journal of the Brazilian Society of Mechanical Sciences and Engineering, 2020. **42**(11): p. 589.
31. Niñerola, R. and E. Giner, *Fracture Toughness of Ti-6Al-4V and Ti-6Al-4V ELI Alloys Fabricated by Electron Beam Melting With Different Orientation and Positions.* Fatigue & Fracture of Engineering Materials & Structures, 2025. **48**(5): p. 2339-2353.